DEVELOPMENT OF SIMPLIFIED CALCULATIONS FOR A MULTIPYRANOMETER ARRAY FOR THE MEASUREMENT OF DIRECT AND DIFFUSE SOLAR RADIATION

Bryce K. Munger,
Mechanical Engineer
Wold Architects and Engineers
St. Paul, Minnisota

Jeff S. Haberl, Ph.D., P.E.
Department of Architecture
Texas A&M University
College Station, Texas

ABSTRACT

This paper describes the development of simplified procedures for a multipyranometer array (MPA) for the continuous measurement of direct and diffuse solar radiation. The MPA described in this paper is an improvement over previously published MPA studies due several new features, including: the incorporation of an artificial horizon that prevents reflected ground radiation from striking the tilted sensors, and a routine that corrects the spectral response of photovoltaic-type sensors used in the MPA. An optimal solution procedure has also been developed that eliminates invalid data which are inherent in the simultaneous solution of the solar equations from the four MPA sensors. In this paper a description of the NIST-traceable calibration facility is provided and results are presented that compare the improved MPA-predicted beam to side-by-side measurements from a precision Normal Incidence Pyrheliometer (NIP).

INTRODUCTION

In the later 1980s several large-scale energy conservation projects were initiated in the United States by utilities and government agencies that incorporated long-term, before-after hourly measurements of energy use, including the Texas LoanSTAR program (Claridge et al. 1991), the Energy Edge project (Diamond et al. 1992), and Pacific Gas and Electric's ACT^2 project (Koran et al. 1992). In these projects the methods used to calculate the measured energy conservation and retrofit savings varied from empirical regression models to calibrated simulation models. In the case where a calibrated simulation model is used to measure the energy retrofit savings it has been shown by Haberl et al. (1995) that the accuracy of a calibrated simulation model can improve substantially when the simulation is driven by a weather file containing locally measured weather data versus calibration efforts that are based on Typical Meteorological Year (TMY) weather data or other standard weather tapes. In buildings where solar effects are significant there is an additional improvement in simulation accuracy when locally-measured beam and diffuse solar measurements are incorporated as well.

Until recently, the long-term recording of beam and diffuse solar measurements usually required either the use of very expensive microprocessor-based precision instruments that tracked the sun, or worse, precision instruments that needed constant manual adjustment to keep them continuously pointed at the sun. In most cases, it is rare to find accurately measured hourly beam and diffuse solar data that extends over several years and does not contain 10% or more missing data due to instrument mis-alignment.

Fortunately, several developments have lead to a relatively inexpensive, robust device that promises to be capable of providing long-term beam and diffuse solar measurements -- the multipyranometer array (MPA). The earliest work on an MPA related device for measuring diffuse sky radiation was performed in Finland by M. Hämäläien et al. (1985). Further development on the MPA was performed in several countries including the United States where Perez (1986) presented a method for deriving beam radiation from a series of vertically mounted pyranometers, and in Israel where Faiman et al. (1988) refined the design of the MPA around four fixed pyranometers and defined a robust solution method that included an anisotropic diffuse sky model. Further advancements were made on the MPA in the United States by Curtiss (1990; 1992; 1993) who investigated different isotropic and anisotropic diffuse sky models, and devised several novel methods for solving the simultaneous MPA equations including an empirically-based statistical model, and artificial neural networks. Curtiss also made several recommendations for improving MPA

measurements, including: (1) corrections for the spectral bias introduced by photovoltaic-based solar sensors, and (2), the suggested use of an artificial horizon to eliminate the ground reflectance term which is unknown.

This paper reports on efforts to develop a simplified MPA calculation including: (1) the addition of a an artificial horizon, and (2) the development of a spectral correction for the photovoltaic-type solar sensor. Also, in the previous work by Curtiss (1990) and in the published MPA dataset that is contained in the ASHRAE Predictor Shootout (Kreider and Haberl 1994a; 1994b) varying amounts of "invalid" data were reported that needed to be filtered-out of the MPA solution without recommendations regarding how to filter these data. This paper reports on the development of a simplified procedure that automatically eliminates invalid data from the simultaneous solution of the solar equations from the four sensors. Results are presented from long-term, side-by-side testing of the MPA-predicted data against measured 15-minute data provided by three precision instruments, including a thermopile-type Precision Spectral Pyranometer (PSP), a Shadow Band Pyranometer (SBP), and a Normal Incidence Pyrheliometer (NIP).

CURRENT WORK

The facility for testing the MPA is located at a university laboratory in central Texas. The test stand is situated on the south side of the laboratory building where the data from the sensors is collected by a data logger which is automatically polled weekly so data can be uploaded into a database[1]. Figure 1 is a photograph of the NIST-traceable test bench that shows the PSP (upper right), SBP, NIP, and MPA (lower left). Uniform black shields were used in back of each sensor to block the reflection from the wall directly to the north of the test stand. Figures 2a and 2b are photographs of the MPA including the proposed artificial horizon. The instrumentation used at the site is listed in Table 1. Additional information about the test stand calibration and data processing routines can be found in Munger (1997).

[1] This data collection effort is part of the LoanSTAR Monitoring program, an eight year $98 million revolving loan program. For additional information on the LoanSTAR program see Claridge et al. (1991). Recently, the solar test facility has been moved to the roof of the College of Architecture where additional testing and refinement can take place.

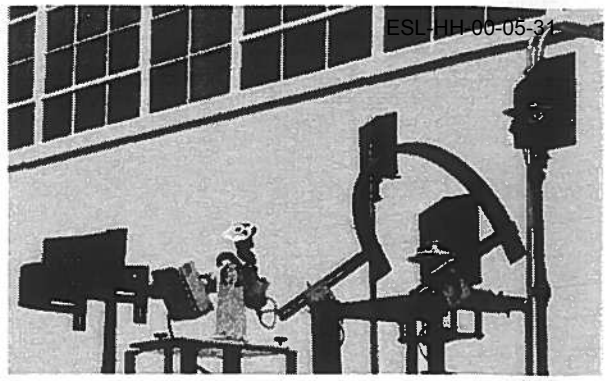

Figure 1: *Solar Test Bench at the Energy Systems Lab*

Table 1*: Instrumentation used at the solar test bench.*

Mfg.	Instrument	Mfg. Stated Accuracy
Eppley Labs	Precision Spectral Pyranometer (PSP)	± 0.5 % from 0-2800 W/ m^2
Eppley Labs	Normal Incidence Pyrheliometer (NIP)	± 0.5 % from 0-2800 W/ m^2
Eppley Labs	Shadow Band with Black & White Pyranometer (SBP)	± 1.0 % from 0-1400 W/ m^2
LI-COR	LI-200SA Pyranometer Sensor	± 3.0 % from 0-3000 W/ m^2

The MPA consists of four photovoltaic-type solar sensors arranged so that each sensor sees a different portion of the sky that corresponds to the sun's path. The arrangement of the sensors in the current MPA is the same as the arrangement used by Curtiss (1990). The MPA that was constructed uses four photovoltaic-type sensors, one sensor mounted horizontally, one 40 degree tilted sensor facing due south, one 40 degree tilted sensor facing 60 degrees east of south, and one 40 degree tilted sensor facing 60 degrees west of south as shown in Figure 2a and 2b. In Figure 2a the MPA is shown with the artificial horizon, in Figure 2b the MPA is shown without the artificial horizon. Both figures provide a view of the blackened shield that is used to uniformly block the reflected sunlight coming from the nearby white wall.

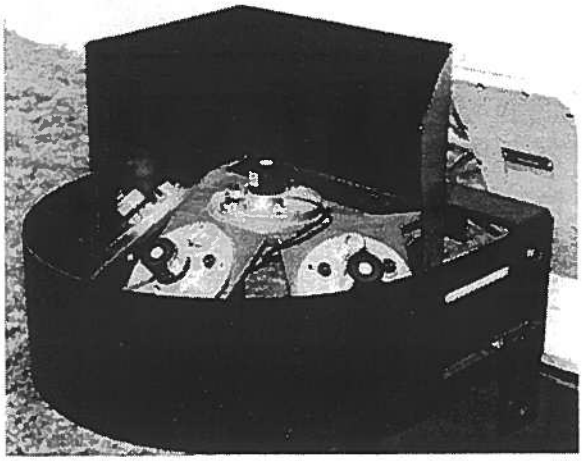

Figure 2a: MPA with Artificial Horizon and Wall Shield

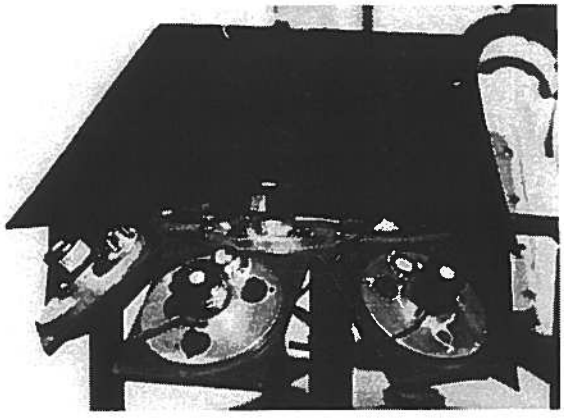

Figure 2b: MPA without Artificial Horizon

In order to test the device, the MPA-calculated beam and diffuse measurements were compared with measured data from NIST-traceable sensors capable of continuously measuring global horizontal radiation, diffuse solar radiation and direct-normal beam radiation. After the initial setup was calibrated and verified the data logger was set to 15-minute integration intervals for long-term measurements. Data quality was maintained through a combination of weekly polling and inspection plots, cross-checking of instrumentation using redundant measurements, and daily visual inspections of the instrumentation alignment (Munger and Haberl 1994, Munger 1997).

RESULTS

The first correction that was developed for the MPA was to adjust for differences in the spectral response of the photovoltaic-type instrumentation used in the MPA and the more accurate NIST-traceable thermopile-type sensor. This difference in spectral response is produced by the different technologies that are used to measure solar radiation. In the precision sensor solar (i.e., the PSP) radiation is proportional to a millivolt output signal that is produced by a thermopile that is measuring the temperature difference between a blackened plate and a reference point within the shaded body of the instrument. A thermopile-type sensor produces a flat response to incident solar radiation. In the photovoltaic-type sensor solar radiation is proportional to the milliamp output produced by a calibrated photovoltaic sensor that is most sensitive to sunlight falling in the 0.5 and 1.0 um range as shown in Figure 3 (Duffie and Beckman 1991). Unfortunately, thermopile-type sensors are expensive, costing approximately five times as much as photovoltaic-type sensors, hence the motivation to use a corrected, photovoltaic-type sensor.

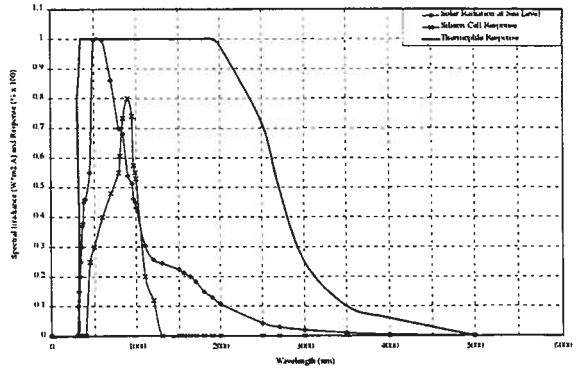

Figure 3: Relative Spectral Response of Thermopile Sensor, and Photovoltaic-type Sensor vs. the Solar Spectrum. (Source: Manufacturer's Manuals).

To correct for the spectral bias of photovoltaic-type sensors in the MPA a simple polynomial correction was developed as shown in Figure 4a, 4b, and 5. Previous efforts in this area by Michalsky et al. (1991) have also developed a more refined method. In general, the effect of the spectral response of the photovoltaic-type sensor is to over-predict solar radiation for insolation levels falling below 600 W/m^2, and under-predict solar radiation for levels above 600 W/m^2. This can be clearly seen in Figure 5 where the mid-day signal from the photovoltaic-

type sensor can be seen dipping below the signal from the PSP. Correcting this with a simple polynomial expression improves the RMSE from 22.48 W/m^2 to 16.77 W/m^2 and improves the R^2 from 99.41% to 99.53 % (Table 2). Figure 4b shows the corrected data from the photovoltaic-type sensor compared against the thermopile-type sensor. Figure 5 shows a daily profile of the data from the PSP along with the corrected and uncorrected data from the photovoltaic sensor.

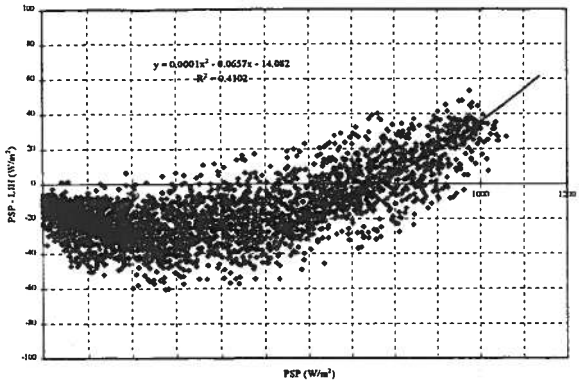

Figure 4a: *PSP vs Photovoltaic-type Sensor Without Spectral Correction.*

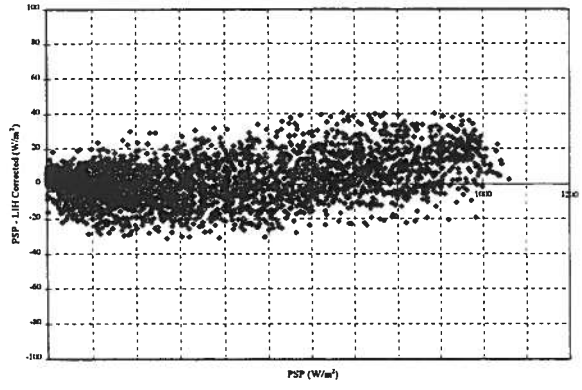

Figure 4b: *PSP vs Photovoltaic-type Sensor With Spectral Correction.*

To obtain beam and diffuse data from the MPA, the equations for the total radiation incident upon each sensor are solved simultaneously for the unknowns. Without any artificial horizon, the system of equations must be solved using three simultaneous equations with three unknowns (i.e. the beam radiation, the diffuse radiation, and the ground-reflected radiation seen by the tilted sensors). As one can see from the

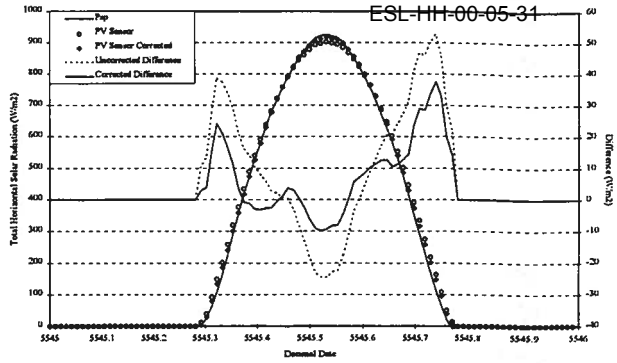

Figure 5: *Global Horizontal Radiation from PSP & Photovoltaic-type Sensor With and Without Spectral Correction. The decimal date in the x-axis represents the number of days since January 1, 1980. For example, 5545 = 3/8/95.*

Table 2: *Comparison of PSP to Photovoltaic-type Sensor Measurements.*

	Without spectral correction	**With spectral correction**
RMSE	22.48 W/m^2	16.77 W/m^2
R^2	99.41 %	99.53%

Note: Data shown are for 4,000 randomly selected data points from 15-minute data taken over a one year period in 1994.

Figures 6a, 6b, and 6c, the solution to the equations is very unstable due to the denominator terms of the equations for the beam radiation wavering back and forth across zero which makes the solution meaningless. Due to this fact, a decision was made to abandon the solution without the artificial horizon and investigate how the solution with the artificial horizon performed.

The next step in the experimentation was to add an artificial horizon as shown in Figure 2a. In the previous work Curtiss (1993) recommended the use of an artificial horizon to eliminate the unknown reflected radiation from the ground. The addition of the artificial horizon reduced the unknown variables to two, (i.e., beam radiation and the diffuse radiation) which creates a somewhat more stable solution as can be seen in Figures 7a, 7b, and 7c.

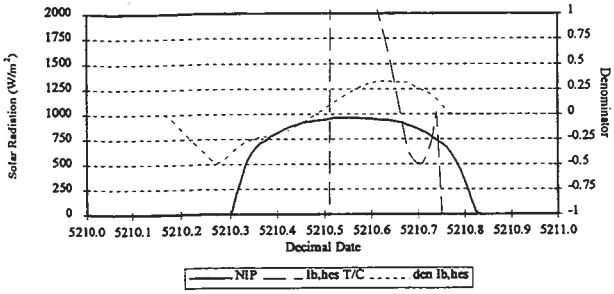

Figure 6a: *Direct Normal Beam Radiation Predicted by Equation 4.37 Using the Horizontal, East, and South MPA Sensors (4/7/94 = decimal date 5210). Data from the NIP and the Denominator of Equation 4.35 are also Shown*

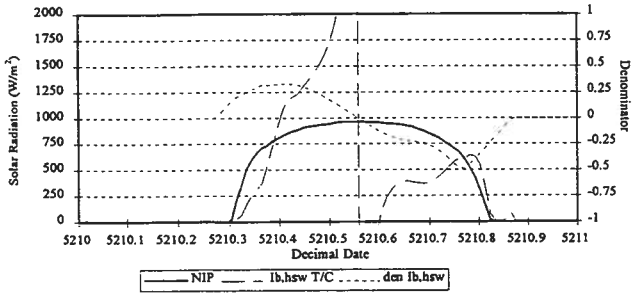

Figure 6b: *Direct Normal Beam Radiation Predicted by Equation 4.37 Using the Horizontal, South, and West MPA Sensors (4/7/94 = decimal date 5210)*

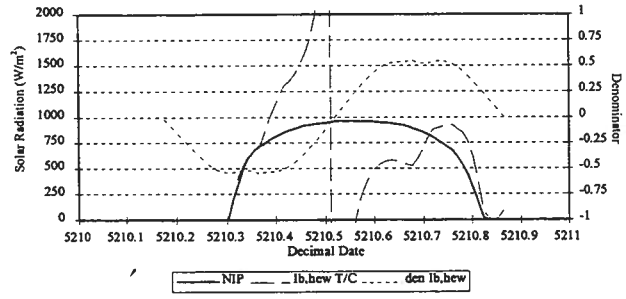

Figure 6c: *Direct Normal Beam Radiation Predicted by Equation 4.37 Using the Horizontal, East, and West MPA Sensors (4/7/94 = decimal date 5210).*

Unfortunately, there were still periods when the solution to the MPA equations for a single pair of sensors produced unstable solutions. These periods are caused by cancellation errors in the geometric tilt factors of the beam and diffuse components. To improve this an additional filtering process was developed that automatically removed the invalid data from the MPA equations as follows. It is observed from Figures 7a, 7b, and 7c that the

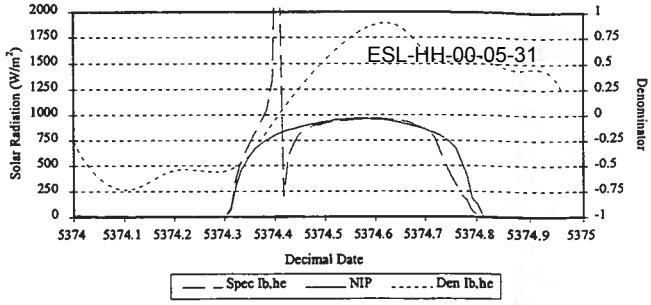

Figure 7a: *Small Number Division with Artificial Horizon (horizontal and east, 9/18/94 = 5374)*

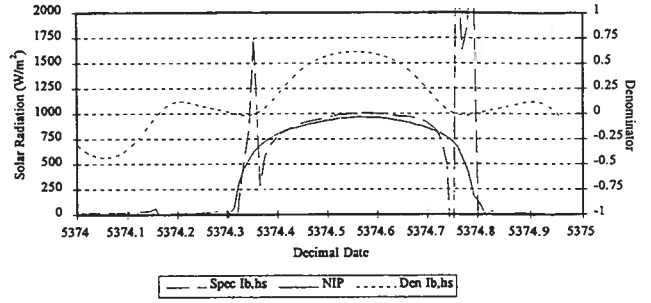

Figure 7b: *Small Number Division with Artificial Horizon (horizontal and south, 9/18/94 = 5374)*

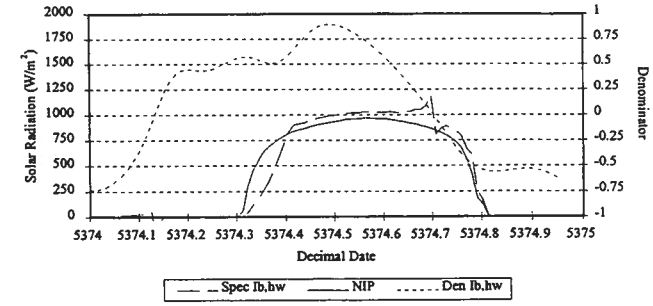

Figure 7c: *Small Number Division with Artificial Horizon (horizontal and west, 9/18/94 = 5374)*

solution becomes physically unreasonable when the denominator approaches zero. However, upon closer inspection it was also observed that at least one pair of sensors offered a valid solution to the MPA equations at any time during the day. Therefore, it was proposed that by "winking" or switching the system of equations a more stable solution could be calculated. The sensor pairs used for the solution were switched based upon the pre-calculated value of the denominators of the individual sensor pairs. To determine the optimal switch point, the solution was performed with varying switch points and the RMSE was calculated for each solution.

Figure 8 shows a plot of the RMSE between the NIP beam and the MPA calculated beam. It can be seen from Figure 8 that a value of 0.175 is the optimal denominator switch point. Therefore, whenever the denominator term of an MPA solution (eqn. 20) was smaller than 0.175 the solution for that pair of sensors was switched off and the other MPA equations were used for that solution. Figure 9a shows the NIP measured direct normal beam radiation and the calculated solutions from each pair of sensors with the switch point set at 0.175. Note that the curves for each solution pair are not continuous over the entire day. This is due to the "winking" of the sensor pairs. This removes the erratic behavior seen in Figures 7a, 7b, and 7c. However, a continuous solution does exist by averaging the prediction from the three pairs, dropping a given pair whenever there is invalid data. It is believed that the invalid data that appear in the Figures 7a, 7b, and 7c are similar to the "invalid data" that was mentioned briefly in Curtis (1990) although no explanation of why the data appear or the method used to remove them was presented in his work.

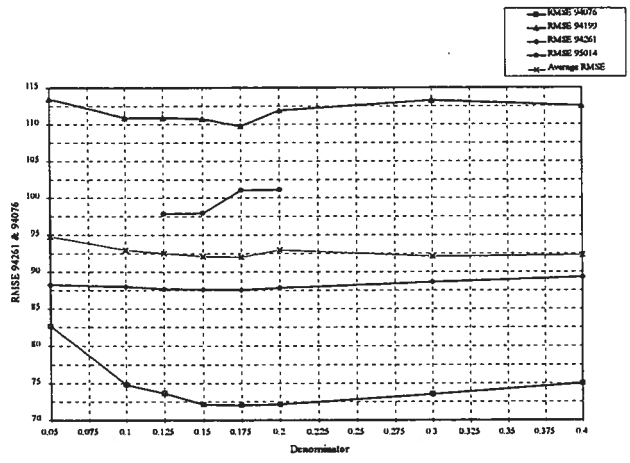

Figure 8: *MPA RMSE*

Figure 9b shows only the NIP measured direct normal beam and the spectrally corrected switched MPA beam solution averaged from all three sensor pairs. The difference between the spectrally switched direct normal beam radiation and the NIP measured direct normal beam radiation is shown in Figure 9c. The two large spikes that represent periods when the MPA underpredicts the beam radiation are believed to be caused by the presence of the white wall located directly to the north of the test bench that blocks the diffuse radiation from the north sky.

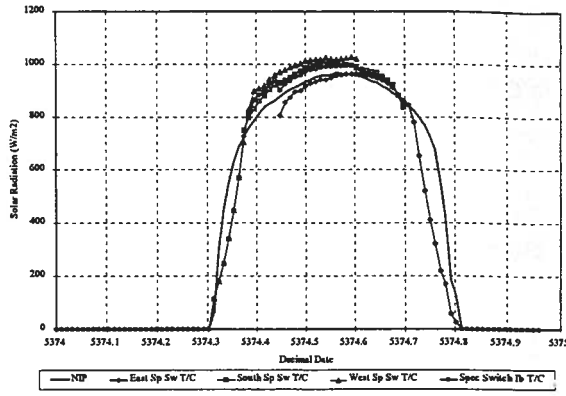

Figure 9a: *Spectrally Switched MPA Calculated Direct Normal Beam Radiation Time Series Plot (9/18/94 = decimal date 5374)*

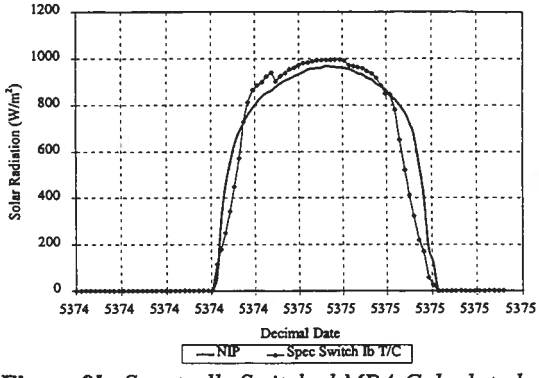

Figure 9b: *Spectrally Switched MPA Calculated Beam Radiation (9/18/94 = decimal date 5374)*

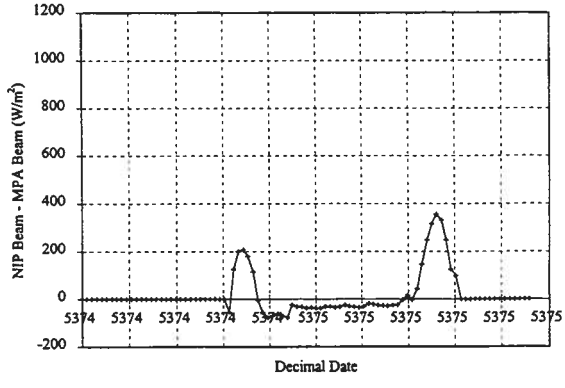

Figure 9c: *Spectrally Switched MPA Calculated Beam Radiation Difference Plot (9/18/94 = decimal date 5374)*

Figures 10a and 10b show MPA predicted beam radiation compared to the beam radiation measured with the NIP. In Figure 10a the data from each set of sensor pairs is summed without any corrections (i.e. no switching or spectral correction) and in Figure 10b the optimized solution to the MPA is shown (i.e. the spectrally corrected, switched solution). It is clear from these plots that the spectrally corrected, switched MPA solution predicts the actual beam radiation measured with the NIP much better than the uncorrected, un-switched solution.

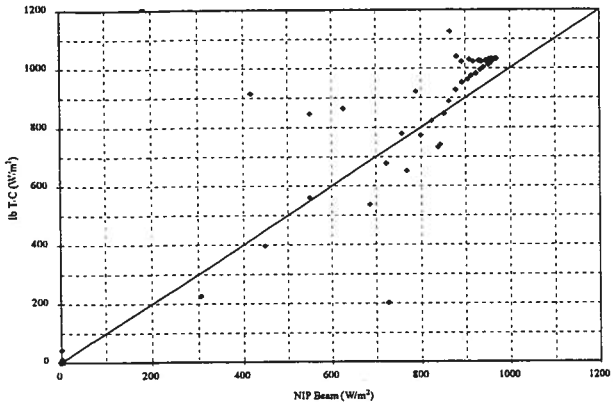

Figure 10a: *Uncorrected MPA Calculated Beam VS NIP Beam with Artificial Horizon (9/18/94 = decimal date 5374)*

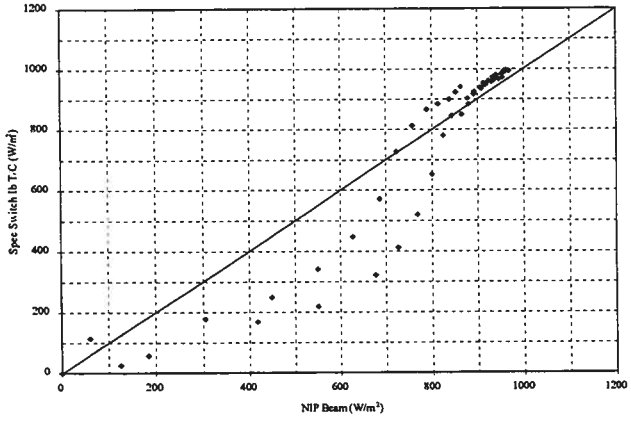

Figure 10b: *Spectrally Switched MPA Calculated Direct Normal Beam Radiation (9/18/94 = decimal date 5374)*

Table 3 shows MPA-predicted beam radiation compared against beam radiation measured by the nearby NIP. In Table 3 results are shown for: a) MPA equations that utilized data directly from the photovoltaic-type sensors without spectral correction (Ib, T/C), b) MPA equations that utilized a spectral correction for the photovoltaic-type sensors (Spec Ib, T/C), c) MPA equations that utilized the invalid data filtering (Switch Ib, T/C), and d) MPA equations that used the spectral correction and invalid data filtering (Spec Switch, Ib, T/C). All MPA equations used the Temps-Coulson (1977) anisotropic diffuse sky model as recommended by Curtiss (1990).

Table 3: *Comparison of MPA-predicted Beam Radiation Against NIP Measurements.*

	Ib, T/C	Spec Ib, T/C	Switch Ib, T/C	Spec Switch Ib, T/C
Spring				
RMSE (W/m²)	272.2	290.6	109.9	111.1
R^2 (%)	70.5	64.2	93.5	93.5
% Invalid (%)	54.0	54.0	0	0
Summer				
RMSE (W/m²)	187.5	178.0	118.5	109.7
R^2 (%)	86.9	93.1	85.5	92.5
% Invalid (%)	16.6	16.6	0	0
Fall				
RMSE (W/m²)	204.4	181.4	100.5	99.2
R^2 (%)	86.9	85.5	93.1	93.2
% Invalid (%)	45.8	45.8	0	0
Winter				
RMSE (W/m²)	938.8	741.4	191.4	97.9
R^2 (%)	70.4	64.1	93.5	95.3
% Invalid (%)	46.2	46.2	0	0
Average				
RMSE (W/m²)	400.7	347.9	130.1	104.5
R^2 (%)	78.7	76.7	91.4	93.6
% Invalid (%)	40.7	40.7	0	0

In Table 3 it can be seen that the combination of a spectral correction and invalid data filtering improved the MPA beam predictions slightly from an RMSE of 113.5 W/m² (previously reported by Curtiss [1990]) to 104.5 W/m². Furthermore, what is most encouraging about the current results is that there is no longer any invalid data in the solution to the MPA equations. This feature, is felt to be a significant enhancement to the MPA development.

SUMMARY AND DISCUSSION

Side-by-side tests of MPA-predicted beam against NIP-measured beam solar radiation have been performed using long term 15-minute data in central Texas. Previously reported work with MPAs has been improved through the addition of a simple artificial horizon, an empirical spectral correction of the signal from the photovoltaic-type sensor, and development of an automated invalid data filtering procedure. These enhancements appear to have

modestly improved the performance of the MPA over the previous results reported by Curtiss, and more significantly, appear to have resolved the issue of the automated removal of invalid data from the solution of the solar equations from the four solar sensors.

Additional testing of the MPA will continue at a new location located on the roof of the College of Architecture at Texas A&M that does not contain any nearby obstructions that plagued the previous location. Potential areas for refinement include optimizing the orientation of the MPA sensors, investigating the use of MPAs for solar beam and diffuse measurements in wildlife management, the use of MPAs for lighting measurements, and development of self-calibration checks for the MPA solar sensors.

ACKNOWLEDGMENTS

Support by the Texas State Energy Conservation Office through the LoanSTAR program is gratefully acknowledged. Special thanks for to the following people at the Energy Systems Lab for their assistance on this project: Dan Turner, Frank Scott, Curtis Boecker, Pat Tollefson, Kelly Milligan, Robert Sparks, and Ron Chambers. Thanks also to Peter Klima and Victor Kootin-Sanwu for assistance with the test bench.

REFERENCES

Claridge, D., Haberl, J., O'Neal, D., Heffington, W., Turner, D., Tombari, C., Roberts, M., Jaeger, S. 1991. "Improving Energy Conservation Retrofits with Measured Results." ASHRAE Journal, Vol.33, No. 10, pp. 14-22, (October).

Curtiss, P. 1990. "An Analysis of Methods for Deriving the Constituent Insolation Components from Multipyranometer Array Measurements," Masters Thesis, Joint Center for Energy Management. (February).

Curtiss, P. 1992. "An Analysis of Methods for Deriving the Constituent Insolation Components from Multipyranometer Array Measurements," Proceedings of the 1992 ASES/JSEE/KSES Solar Energy Engineering Conference, Maui, Hawaii, pp. 109-117.

Curtiss, P. 1993, "An Analysis of Methods for Deriving the Constituent Insolation Components from Multipyranometer Array Measurements," Journal of Solar Energy Engineering, Vol. 115, pp. 11-21. Duffie, J. A. and Beckman, W. A. 1991. Solar Engineering of Thermal Processes, Wiley-Interscience, Madison, Wisconsin.

Diamond, R., Piette, M. Nordman, O., and Harris, J. 1992. "The Performance of the Energy Edge Buildings: Energy Use and Savings," Proceedings of the 1992 ACEEE Summer Study on Energy Efficient Buildings.

Eppley Laboratory, Inc., (1996) 12 Sheffield Ave., P.O. Box 419, Newport, R.I., 02840.

Faiman, D., Zemel, A., and Zangvil, A. 1988. "A method for monitoring Insolation in Remote Regions," Solar Energy, Vol. 39, pp. 327-333.

Haberl, J., Bronson, D., O'Neal, D. 1995. "An Evaluation of the Impact of Using Measured Weather Data Versus TMY Weather Data in a DOE-2 Simulation of an Existing Building in Central Texas." ASHRAE Transactions Technical Paper no. 3921, Vol. 101, Pt. 2, (June).

Hämäläien, M., Nurkkanen, P., and Salen, T., 1985. "A Multisensor Pyranometer for determination of the Direct Component and Angular Distribution of Solar Radiation," Solar Energy, Vol. 35, pp. 511-525.

Koran, W., Kaplan, M. and Steele, T. 1992. "DOE-2.1C Model Calibration With Short-Term Tests versus Calibration With Long-Term Monitored Data," Proceedings of the 1992 ACEEE Summer Study on Energy Efficient Buildings.

Kreider, J. and Haberl, J. 1994a. "Predicting Hourly Building Energy Usage: The Great Energy Predictor Shootout: Overview and Discussion of Results", ASHRAE Transactions Technical Paper, Vol. 100, Pt. 2 (June).

Kreider, J. and Haberl, J. 1994b. "Predicting Hourly Building Energy Usage: The Results of the 1993 Great Energy Predictor Shootout Identify the Most Accurate Method for Making Hourly Energy Use Predictions", ASHRAE Journal, pp. 72-81 (March).

LI-COR Inc. (1996), 4421 Superior St., P. O. Box 4425, Lincoln, NE, 68504.

Michalsky, J., Perez, R., Harrison, L., and LeBaron, B. 1991. "Spectral and Temperature Corrections of Silicon Photovoltaic Solar Radiation Detectors", Solar Energy, Vo. 47, No. 4, pp. 299-305. 5.

Munger, B., Haberl, J. 1994. "An Improved Multipyranometer Array for the Measurement of Direct and Diffuse Solar Radiation", Proceedings of the Ninth Symposium on Improving Building Systems in Hot and Humid Climates, Dallas, TX, pp. 125-131 (May).

Munger, B., Haberl, J. 1997. "An Improved Multipyranometer Array for the Measurement of Direct and Diffuse Solar Radiation", Proceedings of the Clima 2000 Conference, Brussels, Belgium (August).

Munger, B. 1997. "An Improved Multipyranometer Array for the Measurement of Direct and Diffuse Solar Radiation", Master's Thesis, Department of Mechanical Engineering, Texas A&M University, (December).

Perez, R., Seals, R., and Stewart, R. 1986. "On Estimating Beam Irridiance from Vertically Mounted Sensors" Proceedings of the 1986 Annual ASES Meeting, Boulder, Co, pp. 180-183.

Temps, R., and Coulson, J. 1977. "Solar Radiation Incident Upon Slopes of Different Orientations," Solar Energy, Vol. 19, pp. 179-184.

Nomenclature

$I_{T,h}$ = Total radiation measured on the horizontal (W/ m^2)
$I_{T,se}$ = Total radiation measured on the east of south facing tilted surface (W/ m^2)
$I_{T,s}$ = Total radiation measured on the south facing tilted surface (W/ m^2)
$I_{T,sw}$ = Total radiation measured on the west of south facing tilted surface (W/ m^2)
$I_{b,n}$ = Normal beam radiation (W/ m^2)
$I_{d,h}$ = Diffuse radiation measured on the horizontal (W/ m^2)
$R_{b,h}$ = Beam coefficient for horizontal
$R_{b,se}$= Beam coefficient for east of south
$R_{b,s}$= Beam coefficient for south
$R_{b,sw}$= Beam coefficient for west of south
$R_{d,se}$= Diffuse coefficient for east of south
$R_{d,s}$= Diffuse coefficient for south
$R_{d,sw}$= Diffuse coefficient for west of south
$R_{r,se}$= Reflection coefficient for east of south
$R_{r,s}$= Reflection coefficient for south
$R_{r,sw}$= Reflection coefficient for west of south
θ_i = Incidence angle of beam radiation
β = collector tilt angle
γ = off-south azimuth angle
dec = decimal date
n = day of year
ϕ = latitude
ρ = foreground reflectance

δ= declination = $23.45 \times \sin\left(360 \cdot \frac{284+n}{365}\right)$

Hour angle (ω) calculation:

at = 0.001868 · cos(β · π/180)

bt = 0.032077 · sin(β · π/180)

ct = 0.014615 · cos(2 · β · π/180)

dt = 0.04089 · sin(2 · β · π/180)

E = (229.2 · (0.000075+at-bt-ct-dt))

lcorr = ((90-96.55) · 4)

timefix = (lcorr+E)

soldec = dec+(timefix/(24 · 60))

ω = hour angle = $\left(\text{soldec} - \left(\text{int}(\text{soldec}) + 0.5\right)\right) \cdot 24 \cdot 15$

The equation for the total solar radiation incident upon the horizontal MPA sensor is:

$$I_{T,h} = I_{b,n} \cdot R_{b,h} + I_{d,h} \quad (1)$$

The equation for the total solar radiation incident upon the east of south facing tilted MPA sensor is:

$$I_{T,se} = I_{b,n} \cdot R_{b,se} + I_{d,h} \cdot R_{d,se} + I_{T,h} \cdot \rho \cdot R_{r,se} \quad (2)$$

The equation for the total solar radiation incident upon the south facing tilted MPA sensor is:

$$I_{T,s} = I_{b,n} \cdot R_{b,s} + I_{d,h} \cdot R_{d,s} + I_{T,h} \cdot \rho \cdot R_{r,s} \quad (3)$$

The equation for the total solar radiation incident upon the west of south facing tilted MPA sensor is:

$$I_{T,sw} = I_{b,n} \cdot R_{b,sw} + I_{d,h} \cdot R_{d,sw} + I_{T,h} \cdot \rho \cdot R_{r,sw} \quad (4)$$

The beam coefficients (R_b's) are calculated from:

$$R_{b,h} = \cos(\theta_z) = \cos(\theta_{i,h}) \quad (5)$$

$$R_{b,se} = \cos(\theta_{i,se}) \quad (6)$$

$$R_{b,s} = \cos(\theta_{i,s}) \quad (7)$$

$$R_{b,sw} = \cos(\theta_{i,sw}) \quad (8)$$

The diffuse coefficients (R_d's) are calculated from the Temps / Coulson (1977) model and are:

$$R_{d,se} = \frac{1+\cos(\beta_{se})}{2} \cdot \left[1+\sin^3\left(\frac{\beta_{se}}{2}\right)\right] \cdot \left[1+\cos^2\left(\theta_{i,se} \cdot \sin^3(\theta_z)\right)\right] \quad (9)$$

$$R_{d,s} = \frac{1+\cos(\beta_s)}{2} \cdot \left[1+\sin^3\left(\frac{\beta_s}{2}\right)\right] \cdot \left[1+\cos^2\left(\theta_{i,s} \cdot \sin^3(\theta_z)\right)\right] \quad (10)$$

$$R_{d,sw} = \frac{1+\cos(\beta_{sw})}{2} \cdot \left[1+\sin^3\left(\frac{\beta_{sw}}{2}\right)\right] \cdot \left[1+\cos^2\left(\theta_{i,sw} \cdot \sin^3(\theta_z)\right)\right] \quad (11)$$

The incidence angles (θ_i's) in the previous equations are determined from the following:

$$\cos(\theta_z) = \cos(\theta_{i,h}) = \cos(\phi)\cos(\delta)\cos(\omega) + \sin(\phi)\sin(\delta) \quad (12)$$

$$\begin{aligned}\cos(\theta_{i,se}) = {} & \sin(\delta)\sin(\phi)\cos(\beta_{se}) \\ & - \sin(\delta)\cos(\phi)\sin(\beta_{se})\cos(\gamma_{se}) \\ & + \cos(\delta)\cos(\phi)\cos(\beta_{se})\cos(\omega) \\ & + \cos(\delta)\sin(\phi)\sin(\beta_{se})\cos(\gamma_{se})\cos(\omega) \\ & + \cos(\delta)\sin(\beta_{se})\sin(\gamma_{se})\sin(\omega)\end{aligned} \quad (13)$$

$$\begin{aligned}\cos(\theta_{i,s}) = {} & \sin(\delta)\sin(\phi)\cos(\beta_s) \\ & - \sin(\delta)\cos(\phi)\sin(\beta_s)\cos(\gamma_s) \\ & + \cos(\delta)\cos(\phi)\cos(\beta_s)\cos(\omega) \\ & + \cos(\delta)\sin(\phi)\sin(\beta_{se})\cos(\gamma_s)\cos(\omega) \\ & + \cos(\delta)\sin(\beta_s)\sin(\gamma_s)\sin(\omega)\end{aligned} \quad (14)$$

$$\cos(\theta_{i,sw}) = \sin(\delta)\sin(\phi)\cos(\beta_{sw}) - \sin(\delta)\cos(\phi)\sin(\beta_{sw})\cos(\gamma_{sw}) + \cos(\delta)\cos(\phi)\cos(\beta_{sw})\cos(\omega) + \cos(\delta)\sin(\phi)\sin(\beta_{sw})\cos(\gamma_{sw})\cos(\omega) + \cos(\delta)\sin(\beta_{sw})\sin(\gamma_{sw})\sin(\omega) \quad (15)$$

Beam Component Solution

This set of equations are solved to obtain the direct normal beam component ($I_{b,n}$)

Solving the total radiation on the horizontal sensor (eqn 1) for the diffuse component provides:

$$I_{d,h} = I_{T,h} - I_{b,n} \cdot R_{b,h} \quad (16)$$

Inserting this solution into the total on the south east tilted sensor (eqn 2) provides:

$$I_{T,se} = I_{b,n} \cdot R_{b,se} + \left(I_{T,h} - I_{b,n} \cdot R_{b,h}\right) \cdot R_{d,se} + I_{T,h} \cdot \rho \cdot R_r \quad (17)$$

Again, with the horizontal band around the tilted sensors, there is no ground reflection striking the tilted sensors, hence; the $I_{T,h} \cdot \rho \cdot R_r$ term is zero. These equations are in terms of measured quantities only, and can be solved for the direct normal beam radiation ($I_{b,n}$).

Expanding and collecting terms yields:

$$I_{T,se} = I_{b,n} \cdot R_{b,se} + I_{T,h} \cdot R_{d,se} - I_{b,n} \cdot R_{b,h} \cdot R_{d,se} \quad (18)$$

$$I_{b,n} \cdot \left(R_{b,h} \cdot R_{d,se} - R_{b,se}\right) = I_{T,h} \cdot R_{d,se} - I_{T,se} \quad (19)$$

Solving for the direct normal beam radiation using the horizontal and east MPA sensors ($I_{bn,he}$) yields:

$$I_{bn,he} = \frac{I_{T,h} \cdot R_{d,se} - I_{T,se}}{R_{b,h} \cdot R_{d,se} - R_{b,se}} \quad (20)$$

We now have an equation for the beam component of the total radiation on the horizontal which utilizes measured data from the east of south tilted sensor and the horizontal sensor. This same procedure is applied to each of the other tilted sensors in turn which yields three values of $I_{bn,xx}$. The equations for $I_{bn,xx}$ from the MPA with the artificial horizon in place are:

The solution for $I_{b,n}$ from the horizontal sensor and the tilted south sensor is:

$$I_{bn,hs} = \frac{I_{T,h} \cdot R_{d,s} - I_{T,s}}{R_{b,h} \cdot R_{d,s} - R_{b,s}} \quad (21)$$

The solution for $I_{b,n}$ from the horizontal sensor and the tilted south west sensor is:

$$I_{bn,hw} = \frac{I_{T,h} \cdot R_{d,sw} - I_{T,sw}}{R_{b,h} \cdot R_{d,sw} - R_{b,sw}} \quad (22)$$